INTERNATIONAL JOURNAL FOR NUMERICAL METHODS IN FLUIDS, VOL. 2, 89–112 (1982)

SELECTIVE LUMPING FINITE ELEMENT METHOD FOR SHALLOW WATER FLOW

MUTSUTO KAWAHARA, HIROKAZU HIRANO AND KHOJI TSUBOTA

Department of Civil Engineering, Chuo University, Kasuga, Bunkyo-ku, Tokyo, Japan

KAZUO INAGAKI

Technical Research Division, Unic Corporation, Shinjuku, Shinjuku-ku, Tokyo, Japan

SUMMARY

A finite element method for solving shallow water flow problems is presented. The standard Galerkin method is employed for spatial discretization. The numerical integration scheme for the time variation is the explicit two step scheme, which was originated by the authors and their co-workers. However, the original scheme has been improved to remove the erroneous artifical damping effect. Since the improved scheme employs a combination of lumped and unlumped coefficients, the scheme is referred to as a selective lumping scheme. Stability conditions and accuracy are investigated by considering several numerical examples. The method has been applied to the tidal flow in Osaka Bay and Yatsushiro Bay.

KEY WORDS Two Step Scheme Selective Lumping Method Tidal Flow Osaka Bay

INTRODUCTION

In the analysis of the unsteady shallow water flow by the finite element method, it is always necessary to introduce a numerical integration procedure for the time function. A large number of integration methods have been presented in the literature and these can be classified into three categories. The first is the method which will employ an analytical solution.[1–3] However, in practice, this is severely restricted in application. The second is the method which employs constituent decomposition such as a Fourier analysis and is usually applied in tidal modelling.[4–12] The third, which is the most widely used method, is referred to as the time marching method. This is a numerical integration procedure in which total time to be analysed is divided into a large number of very short time intervals associated with discrete times and the numerical integration is carried out for each time interval using the numerical values calculated previously.

The time marching schemes can be grouped into two categories, namely, the implicit scheme,[13–49] which requires the procedures to solve an algebraic simultaneous equation system, and the explicit scheme,[50–66] which does not require the procedure. It is noted that in general computations conducted using the implicit scheme are more stable than for the explicit scheme. However, the computational times for implicit schemes are usually quite large when solving an algebraic simultaneous equation system. To save computational time in an implicit scheme, a numerical integration based on a topologically regular finite element arrangement has been presented.[13,14] However, this topologically regular arrangement is not

0271–2091/82/010089–24$02.40

Received 25 February 1981
Revised 23 June 1981

useful for practical problems. Moreover, the computational time for each time cycle in the explicit scheme is far shorter than that in the implicit scheme although the time increment chosen should be shorter. The core storage requirement in the explicit scheme is also much less than that in the implicit scheme. In addition, for several coastal sea models, especially in tidal modelling, a secondary wave is apparent which has a higher frequency than that of the wave incident at the boundary. These higher modes are induced by the effect of irregular configuration of the coastline and bottom topography. For these problems, it is dangerous to use the implicit scheme since the selection of a long time increment sometimes misses the higher frequency mode. Considering the above-mentioned items, the explicit numerical integration in time could be concluded to be much more preferable for practical computations.

The numerical integration scheme employed in this paper is the explicit two step scheme. The original scheme has been presented by Kawahara *et al.*[55–62] After several observations, it was concluded that the numerical results obtained by the original scheme include slight artifical damping.[25] Therefore, in this paper, the scheme has been improved to remove this erroneous artifical damping effect. The improved scheme is referred to as the 'selective lumping two step explicit scheme'. It is necessary to investigate the numerical property of the scheme before applying it to practical problems. For this purpose, the stability and damping properties of the selective lumping two step scheme have been tested using the one-dimensional shallow water equation with the damping effect being evaluated empirically. Following this, the numerical results obtained using the selective lumping scheme have been compared with the observed data obtained from an Osaka Bay model. It can be concluded that the numerical damping effect in computations using the improved scheme is insignificant and that the numerical procedure is simple and stable. The finite element method using the selective lumping two step explicit scheme has been applied to analysis of tidal flats in Yatsushiro Bay, Japan.

BASIC EQUATIONS

It is commonly known that the behaviour of current flow in estuaries and coastal seas can be expressed by the shallow water flow equation. Assuming the density of water is constant, the basic equations can be derived from the three-dimensional Navier–Stokes equation by integrating over the water depth and assuming hydrostatic pressure. The equation of motion and the equation of continuity can be described in the following form

$$\frac{\partial u_i}{\partial t} + u_j u_{i,j} + g\zeta_{,i} - A_l(u_{i,j} + u_{j,i})_{,j} + \tau_i^B = 0 \tag{1}$$

$$\frac{\partial \zeta}{\partial t} + \{(H+\zeta)u_i\}_{,i} = 0 \tag{2}$$

where u_i and ζ represent the vertically averaged velocity and water elevation from the mean sea level, and g, H, A_l are gravity acceleration, water depth, eddy viscosity respectively. The bottom fricition τ_i^B is assumed by the Chezy formula as

$$\tau_i^B = \frac{g}{C^2} u_i (u_k u_k)^{1/2} \tag{3}$$

where C is a Chezy coefficient. Coriolis forces and surface friction are, for simplicity, both

ignored. Here and henceforth, indicial notation is used and the usual summation convention with repeated indices is employed.

Four types of condition are introduced, viz, the conditions for velocity, surface flux, surface discharge and water elevation. On the boundary S_1, the velocity is postulated in the form

$$u_i = \hat{u}_i \quad \text{on } S_1 \tag{4}$$

where superscripted $\hat{}$ means the value which is specified on the boundary. On the boundary S_2, a surface flux is assumed

$$r_i = A_l(u_{i,j} + u_{j,i})n_j = \hat{r}_i \quad \text{on } S_2 \tag{5}$$

where n_j are the components of the unit normals to the boundary. A surface discharge is specified on boundary S_3,

$$q = (H+\zeta)u_i n_i = \hat{q} \quad \text{on } S_3 \tag{6}$$

and the water elevation is given on the boundary S_4,

$$\zeta = \hat{\zeta} \quad \text{on } S_4 \tag{7}$$

The whole boundary S of the domain V to be analysed is assumed to consist of S_1 and S_2 with

$$\begin{aligned} S_1 \cap S_2 &= \varnothing \\ S_1 \cup S_2 &= S \end{aligned} \tag{8}$$

where $\varnothing$ is the null set. For the boundary S_3 and S_4, a similar relation is introduced,

$$\begin{aligned} S_3 \cap S_4 &= \varnothing \\ S_3 \cup S_4 &= S \end{aligned} \tag{9}$$

The precise discussions on the natural boundary conditions are described by Kawahara.[58]

FINITE ELEMENT FORMULATION

The standard Galerkin finite element method is employed for the spatial discretization and the flow field to be analysed is divided into small regions called finite elements. Multiplying both sides of equations (1) and (2) by weighting functions u_i^* and ζ^* and integrating over the domain V, the weighted residual equations can be derived in the form

$$\int_V \left(u_i^* \frac{\partial u_i}{\partial t}\right) \mathrm{d}V + \int_V (u_i^* u_j u_{i,j})\,\mathrm{d}V + \int_V (u_i^* g\zeta_{,i})\,\mathrm{d}V + \int_V A_l(u_{i,j}^* u_{j,i})\,\mathrm{d}V + \int_V A_l(u_{i,j}^* u_{i,j})\,\mathrm{d}V + \int_V (u_i^* \tau_i^{\mathrm{B}})\,\mathrm{d}V = \int_{S_2} (u_i^* \hat{r}_i)\,\mathrm{d}s \tag{10}$$

$$\int_V \left(\zeta^* \frac{\partial \zeta}{\partial t}\right) \mathrm{d}V - \int_V \{\zeta_{,i}^* (H+\zeta)u_i\}\,\mathrm{d}V = \int_{S_3} (\zeta^* \hat{q}_i)\,\mathrm{d}S \tag{11}$$

Current velocity components, water elevation and their corresponding weighting functions are interpolated in each finite element as follows

$$u_i = \Phi_\alpha u_{\alpha i}, \qquad u_i^* = \Phi_\alpha u_{\alpha i}^* \tag{12), (13}$$

$$\zeta = \Phi_\alpha \zeta_\alpha, \qquad \zeta^* = \Phi_\alpha \zeta_\alpha^* \tag{14), (15}$$

where Φ_α denotes the interpolation function for velocity or water elevation and $u_{\alpha i}$, ζ_α are the mean velocity and water elevation at the αth node of each finite element, $u^*_{\alpha i}$, ζ^*_α are the nodal values of the weighting function for each finite element. For the interpolation functions, standard linear functions based on the three node triangular finite element are used.

The Galerkin procedure leads, upon substituting equations (12)–(15) into equations (10) and (11), to the following finite element equation

$$M_{\alpha\beta}\dot{u}_{\beta i} + K_{\alpha\beta\gamma j}u_{\beta j}u_{\gamma i} + N_{\alpha i\beta}\zeta_\beta + S_{\alpha i\beta j}u_{\beta j} = 0 \tag{16}$$

$$M_{\alpha\beta}\dot{\zeta}_\beta + A_{\alpha\beta j\gamma}u_{\beta j}\zeta_\gamma + B_{\alpha\beta j}u_{\beta j} = 0 \tag{17}$$

where

$$M_{\alpha\beta} = \int_V (\Phi_\alpha \Phi_\beta)\,\mathrm{d}V$$

$$K_{\alpha\beta\gamma j} = \int_V (\Phi_\alpha \Phi_{\beta,j} \Phi_\gamma)\,\mathrm{d}V$$

$$N_{\alpha i\beta} = \int_V g(\Phi_\alpha \Phi_{\beta,i})\,\mathrm{d}V$$

$$S_{\alpha i\beta j} = \int_V A_l(\Phi_{\alpha,i}\Phi_{\beta,j})\,\mathrm{d}V + \int_V A_l(\Phi_{\alpha,k}\Phi_{\beta,k})\delta_{ij}\,\mathrm{d}V + \int \frac{g}{C^2}(u_k u_k)^{1/2}\cdot(\Phi_\alpha\Phi_\beta)\delta_{ij}\,\mathrm{d}V$$

$$A_{\alpha\beta j\gamma} = \int_V (\Phi_{\alpha,j}\Phi_\beta\Phi_\gamma)\,\mathrm{d}V$$

$$B_{\alpha\beta j} = A_{\alpha\beta\gamma j}\cdot H_\gamma$$

where the bottom friction term is linearized and the water depth at each finite element is interpolated as

$$H = \Phi_\alpha H_\alpha \tag{18}$$

in which H_α denotes the water depth at each nodal point of the finite element. The Kronecker delta function is denoted by δ_{ij}.

Superposing equations (16) and (17) for all nodal points in the whole flow field, the final finite element equation can be derived as a non-linear first order simultaneous differential equation system.

SELECTIVE LUMPING FINITE ELEMENT METHOD

The finite element equation discretized in terms of the spatial function can be expressed in the form

$$M_{\alpha\beta}\dot{V}_\beta + K_{\alpha\beta\gamma}V_\beta V_\gamma + N_{\alpha\beta}Z_\beta + S_{\alpha\beta}V_\beta = 0 \tag{19}$$

$$M_{\alpha\beta}\dot{Z}_\beta + A_{\alpha\beta\gamma}V_\beta Z_\gamma + B_{\alpha\beta}Z_\beta = 0 \tag{20}$$

where V_β and Z_β denote the velocity and water surface elevation at all nodal points in the flow field. The coefficients of equations (19) and (20) can be derived by the superposition of equations (16) and (17).

To solve equations (19) and (20), it is necessary to introduce a numerical integration scheme in time. The integration scheme employed in this paper, as stated previously, is

referred to as the selective lumping two step explicit scheme. The original scheme has been presented by Kawahara *et al.*[55–62] The total time to be analysed is divided into a number of discrete time points, one of which is denoted by nth time point. The short time interval between the nth and $(n+1)$th time points is expressed by Δt. The selective lumping scheme could be divided into two methods, depending on whether the basic equations include the viscosity term or not.

In the case when the finite element equations include the viscosity term, the selective lumping scheme can be expressed as follows for the first step

$$\bar{M}_{\alpha\beta} V_\beta^{n+\frac{1}{2}} = \bar{M}_{\alpha\beta} V_\beta^n - \frac{\Delta t}{2}(K_{\alpha\beta\gamma} V_\beta^n V_\gamma^n + N_{\alpha\beta} Z_\beta^n + S_{\alpha\beta} V_\beta^n) \tag{21}$$

$$\bar{M}_{\alpha\beta} Z_\beta^{n+\frac{1}{2}} = \bar{M}_{\alpha\beta} Z_\beta^n - \frac{\Delta t}{2}(A_{\alpha\beta\gamma} V_\beta^n Z_\gamma^n + B_{\alpha\beta} Z_\beta^n) \tag{22}$$

and for the second step

$$\bar{M}_{\alpha\beta} V_\beta^{n+1} = \bar{M}_{\alpha\beta} V_\beta^n - \Delta t(K_{\alpha\beta\gamma} V_\beta^{n+\frac{1}{2}} V_\gamma^{n+\frac{1}{2}} + N_{\alpha\beta} Z_\beta^{n+\frac{1}{2}} + S_{\alpha\beta} V_\beta^n) \tag{23}$$

$$\bar{M}_{\alpha\beta} Z_\beta^{n+1} = \bar{M}_{\alpha\beta} Z_\beta^n - \Delta t(A_{\alpha\beta\gamma} V_\gamma^{n+\frac{1}{2}} Z_\gamma^{n+\frac{1}{2}} + B_{\alpha\beta} Z_\beta^{n+\frac{1}{2}}) \tag{24}$$

where superscripted n denotes the value at the nth time point. The overbar $\bar{}$ on the coefficient $\bar{M}_{\alpha\beta}$ expresses the lumped coefficient and $\tilde{M}_{\alpha\beta}$ is the selective lumping coefficient:

$$\tilde{M}_{\alpha\beta} = e\bar{M}_{\alpha\beta} + (1-e)M_{\alpha\beta} \tag{25}$$

i.e. the coefficient derived from a combination of the lumped and unlumped coefficients. In equation (25), the parameter e expresses the ratio of the lumped coefficient, which is referred to as the selective lumping parameter. The technique expressed in equations (21)–(24) using $\tilde{M}_{\alpha\beta}$ is found to stabilize the numerical integration in time and to reduce considerably the artificial damping effect. If the selective lumping parameter e is chossen to be zero, the scheme is exactly coincident with the original scheme presented by Kawahara *et al.*[55–62]

For the case when the finite element equations exclude the viscosity term, it is necessary to modify the selective lumping scheme as follows:
for the first step

$$\bar{M}_{\alpha\beta} V_\beta^{n+\frac{1}{2}} = \tilde{M}_{\alpha\beta} V_\beta^n - \frac{\Delta t}{2}(K_{\alpha\beta\gamma} V_\beta^n V_\gamma^n + N_{\alpha\beta} Z_\beta^n) \tag{26}$$

$$\bar{M}_{\alpha\beta} Z_\beta^{n+\frac{1}{2}} = \tilde{M}_{\alpha\beta} Z_\beta^n - \frac{\Delta t}{2}(A_{\alpha\beta\gamma} V_\beta^n Z_\gamma^n + B_{\alpha\beta} Z_\beta^n) \tag{27}$$

and for the second step

$$\bar{M}_{\alpha\beta} V_\beta^{n+1} = \tilde{M}_{\alpha\beta} V_\beta^n - \Delta t(K_{\alpha\beta\gamma} V_\beta^{n+\frac{1}{2}} V_\gamma^{n+\frac{1}{2}} + N_{\alpha\beta} Z_\beta^{n+\frac{1}{2}}) \tag{28}$$

$$\bar{M}_{\alpha\beta} Z_\beta^{n+1} = \tilde{M}_{\alpha\beta} Z_\beta^n - \Delta t(A_{\alpha\beta\gamma} V_\beta^{n+\frac{1}{2}} Z_\gamma^{n+\frac{1}{2}} + B_{\alpha\beta} Z_\beta^{n+\frac{1}{2}}) \tag{29}$$

The scheme depicted by equations (21)–(24) is used when the viscosity term is neglected; the scheme, unfortunately, turns out to be unstable. Therefore, it is necessary to introduce the stablizing technique in equations (21) and (23). The selective lumping scheme in equations (26)–(29) is thus derived.

STABILITY CONSIDERATION

The CFL stability condition of the selective lumping scheme is argued for the one dimensional linear shallow water equation. The basic equation is written as

$$\frac{\partial u}{\partial t}+g\frac{\partial \zeta}{\partial x}=0 \tag{30}$$

$$\frac{\partial \zeta}{\partial t}+H\frac{\partial u}{\partial x}=0 \tag{31}$$

where u and ζ represent the velocity and water elevation and g, H are the acceleration due to gravity and water depth, respectively. The water depth H is assumed for simplicity to be constant for the whole domain. Introducing a linear interpolation function for each finite element of length Δx, the finite element equation can be described in the following form.

$$M_{\alpha\beta}\dot{u}_\beta + gS_{\alpha\beta}\zeta_\beta = 0 \tag{32}$$

$$M_{\alpha\beta}\dot{\zeta}_\beta + HS_{\alpha\beta}u_\beta = 0 \tag{33}$$

where u_β and ζ_β denote the velocity and water elevation at βth node of the finite element and

$$M_{\alpha\beta}=\begin{pmatrix}\frac{\Delta x}{3} & \frac{\Delta x}{6}\\ \frac{\Delta x}{6} & \frac{\Delta x}{3}\end{pmatrix} \qquad S_{\alpha\beta}=\begin{pmatrix}-\frac{1}{2} & \frac{1}{2}\\ -\frac{1}{2} & \frac{1}{2}\end{pmatrix}$$

The lumped and the selective lumping coefficients are expressed as follows.

$$\bar{M}_{\alpha\beta}=\begin{pmatrix}\frac{\Delta x}{2} & \\ & \frac{\Delta x}{2}\end{pmatrix} \qquad \tilde{M}_{\alpha\beta}=\begin{pmatrix}\frac{2+e}{6}\Delta x & \frac{1-e}{6}\Delta x\\ \frac{1-e}{6}\Delta x & \frac{2+e}{6}\Delta x\end{pmatrix}$$

Superposing equations (32) and (33), the selective lumping finite element scheme for the ith nodal point can be written as:
for the first step

$$u_i^{n+\frac{1}{2}}=\left(\frac{1-e}{6}\right)u_{i-1}^n+\left(\frac{2+e}{3}\right)u_i^n+\left(\frac{1-e}{6}\right)u_{i+1}^n-\frac{\mu}{2}g\left\{\left(-\frac{1}{2}\right)\zeta_{i-1}^n+\left(\frac{1}{2}\right)\zeta_{i+1}^n\right\} \tag{34}$$

$$\zeta_i^{n+\frac{1}{2}}=\left(\frac{1-e}{6}\right)\zeta_{i-1}^n+\left(\frac{2+e}{3}\right)\zeta_i^n+\left(\frac{1-e}{6}\right)\zeta_{i+1}^n-\frac{\mu}{2}H\left\{\left(-\frac{1}{2}\right)u_{i-1}^n+\left(\frac{1}{2}\right)u_{i+1}^n\right\} \tag{35}$$

and for the second step

$$u_i^{n+1}=\left(\frac{1-e}{6}\right)u_{i-1}^n+\left(\frac{2+e}{3}\right)u_i^n+\left(\frac{1-e}{6}\right)u_{i+1}^n-\mu g\left\{\left(-\frac{1}{2}\right)\zeta_{i-1}^{n+\frac{1}{2}}+\left(\frac{1}{2}\right)\zeta_{i+1}^{n+\frac{1}{2}}\right\} \tag{36}$$

$$\zeta_i^{n+1}=\left(\frac{1-e}{6}\right)\zeta_{i-1}^n+\left(\frac{2+e}{3}\right)\zeta_i^n+\left(\frac{1-e}{6}\right)\zeta_{i+1}^n-\mu H\left\{\left(-\frac{1}{2}\right)u_{i-1}^{n+\frac{1}{2}}+\left(\frac{1}{2}\right)u_{i+1}^{n+\frac{1}{2}}\right\} \tag{37}$$

where

$$\mu=\frac{\Delta t}{\Delta x}. \tag{38}$$

Consider the solution of the type

$$u_i^n = R^n \exp(j\omega i) \tag{39}$$

$$\zeta_i^n = S^n \exp(j\omega i) \tag{40}$$

where j is the imaginary unit and R, S are the amplification factors of velocity and water elevation respectively. Introducing equations (39) and (40) into equations (34)–(37) and rearranging the terms, the following equation can be derived.

$$\begin{pmatrix} R^{n+\frac{1}{2}} \\ S^{n+\frac{1}{2}} \\ \hline R^{n+1} \\ S^{n+1} \end{pmatrix} = \left(\begin{array}{cc:cc} a & \frac{1}{2}gb & & \\ \frac{1}{2}Hb & a & & \\ \hdashline a & & & gb \\ & a & Hb & \end{array}\right) \cdot \begin{pmatrix} R^n \\ S^n \\ \hline R^{n+\frac{1}{2}} \\ S^{n+\frac{1}{2}} \end{pmatrix} \tag{41}$$

where

$$a = \frac{2+e}{3} + \frac{1-e}{3}\cos\omega$$

$$b = -j\mu \sin\omega$$

The CFL stability condition can be obtained from equation (41) by using the fact that the eigenvalues of the coefficient matrix should be less than 1. The result is

$$\mu = \frac{\Delta t}{\Delta x} \leqq \frac{\sqrt{2} - \frac{e}{\sqrt{2}}}{3} \cdot \frac{1}{\sqrt{(gH)}} \tag{42}$$

Equation (42) indicates how to choose the time increment Δt. The time increment should be chosen to be as long as possible whilst maintaining stability. Several numerical computations indicate that the numerical damping effect was minimum for maximum Δt.

If e is equal to 0 equation (42) turns out to be the criterion in the case of the original two step explicit scheme. Apparently, the original scheme is associated with the longest Δt but the accuracy is less. Even if e is chosen to be 1, the computation is still stable but the scheme should use the shortest time increment. Actually, in a practical computation, it is necessary to employ $0{\cdot}95 > e > 0{\cdot}8$. From the authors' numerical experiments, a selective lumping parameter e within these limits does not give rise to erroneous numerical damping.

NUMERICAL TEST EXAMPLE

The first example is the analysis of a solitary wave propagated along a one-dimensional channel with uniform bottom slope. The finite element idealization and the initial configuration of the solitary wave is shown in Figure 1. Although the deformation phenomenon is limited to one-dimensional behaviour, the analysis has been performed using the two-dimensional computer program. The number of subdivisions illustrated in Figure 1 is denoted by N, i.e. the finite element mesh with $N = 40$ is shown in Figure 1.

The computed results are represented in Figures 2–5. In Figure 2, the numerical results obtained by the original two step explicit scheme (i.e. the lumping parameter $e = 0$) are plotted. The qualitative behaviour of the analytical solution indicates that the peak value gradually becomes higher as the solitary wave approaches the shallower domain. In the case when the number of subdivisions is not large enough (e.g. $N = 40$ or 80), a completely dissipated solitary wave has been computed. This is contrary to the expected behaviour. The

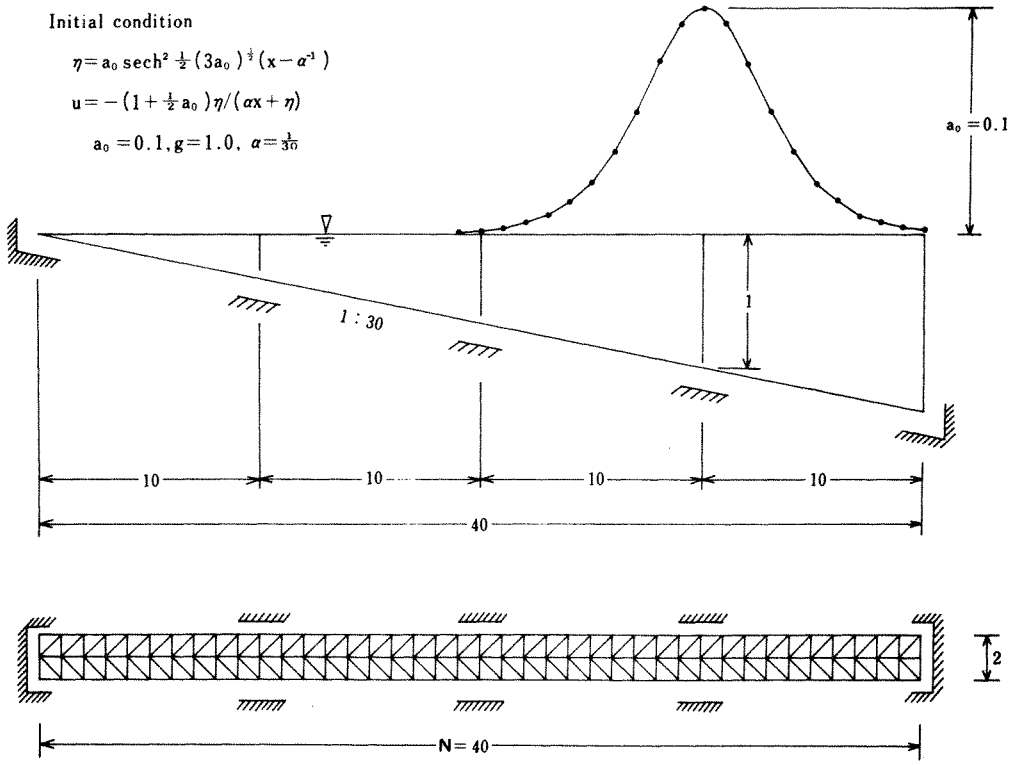

Figure 1. Finite element idealization of channel and initial condition

computed results seem to include a significant damping effect. Furthermore, as the number of subdivisions is increased (e.g. $N = 160$ or 320) then the results seem to improve. However, the peak values are still lower than those of the exact solution. The final peak value of the analytical linear solution is 1·2 times the initial peak value. In the above computations, the time increment Δt is chosen to be as long as possible but within the limit where stable computations are obtained.

In Figure 3, the numerical results using the selective lumping parameter $e = 0{\cdot}6$ are presented. The numerical damping effect is still apparent in this example. However, as the number of subdivisions is increased, it is seen that the numerical results can be improved. In the computations in Figures 2 and 3 and also the following figures, the time increment Δt is chosen to be shorter as the number of subdivision grows larger.

Figure 4 shows the numerical results obtained using the selective lumping parameter $e = 0{\cdot}8$. In the case when the number of subdivisions is not large enough ($N = 40$ or 80), the computed results do not coincide with the analytical solution. On the other hand, using the number of subdivisions $N = 160$ or 320, the computed solitary waves are close to the analytical solution. Therefore, it is seen that the lumping parameter e should be used larger than 0·8 and the refined finite element mesh should also be employed. It can be deduced that the finite element mesh should be such that at least 40 nodal points should be included in one half wave. It is slightly regrettable but notable that the time increment Δt is the shortest in the case when $e = 0{\cdot}8$ and $N = 320$.

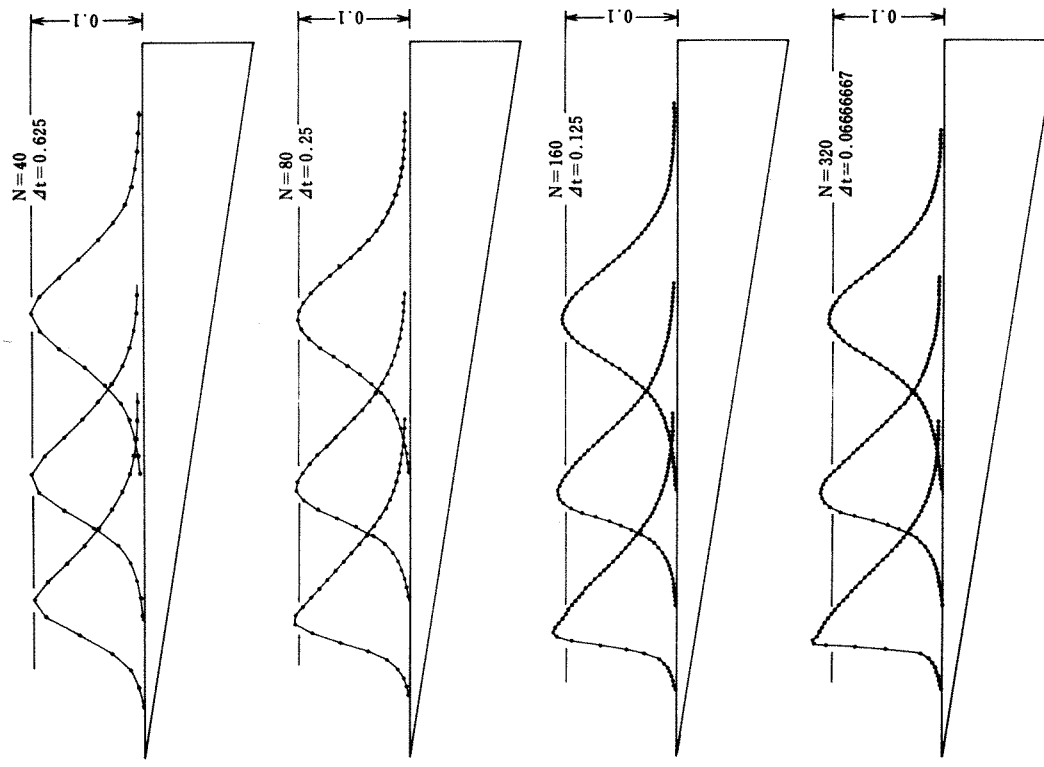

Figure 3. Computed water elevation by the scheme $e = 0{\cdot}6$

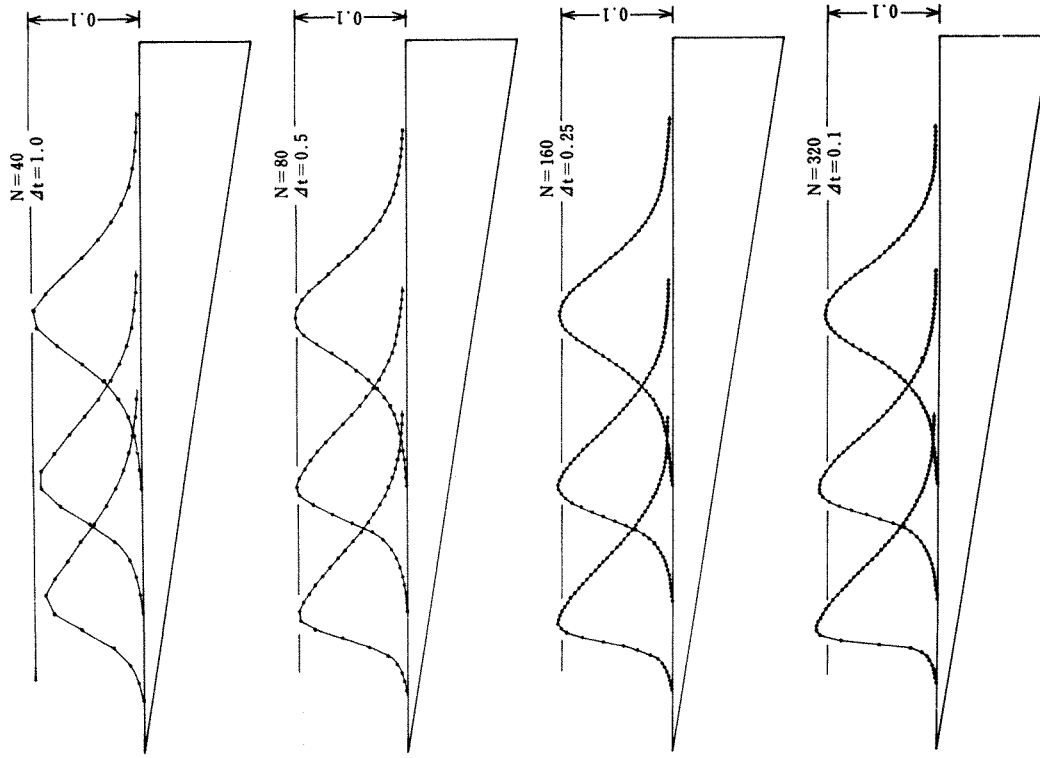

Figure 2. Computed water elevation by the original scheme ($e = 0{\cdot}0$)

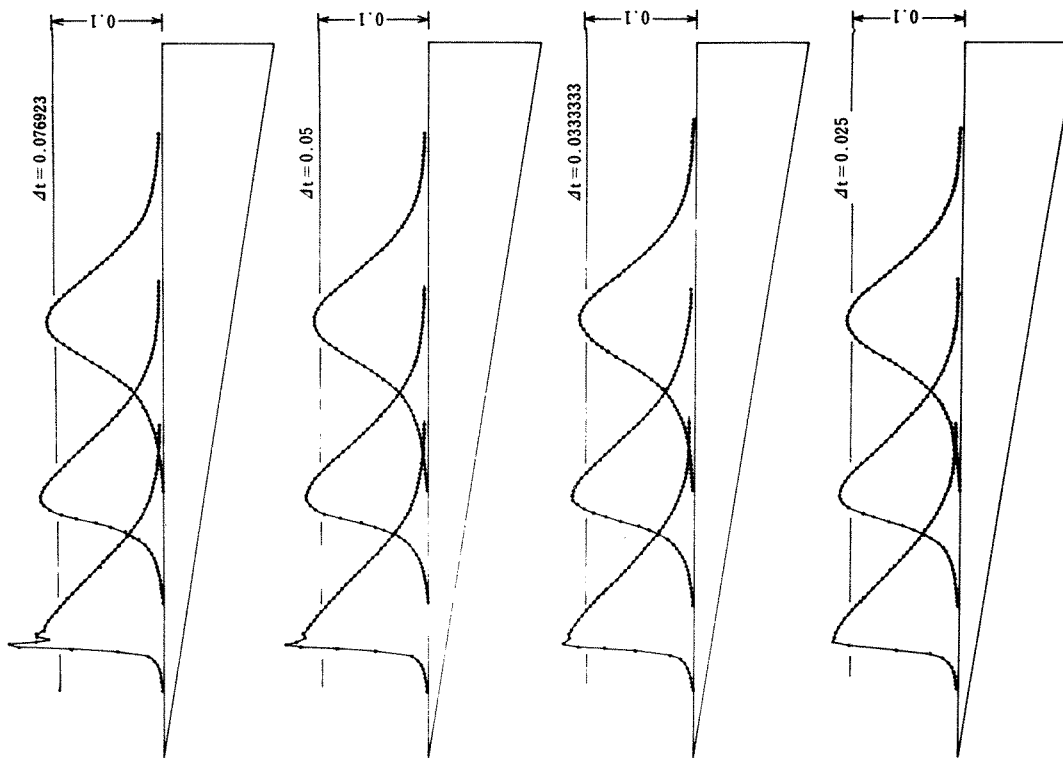

Figure 5. Computed water elevation by the scheme $N = 320$ and $e = 0{\cdot}8$

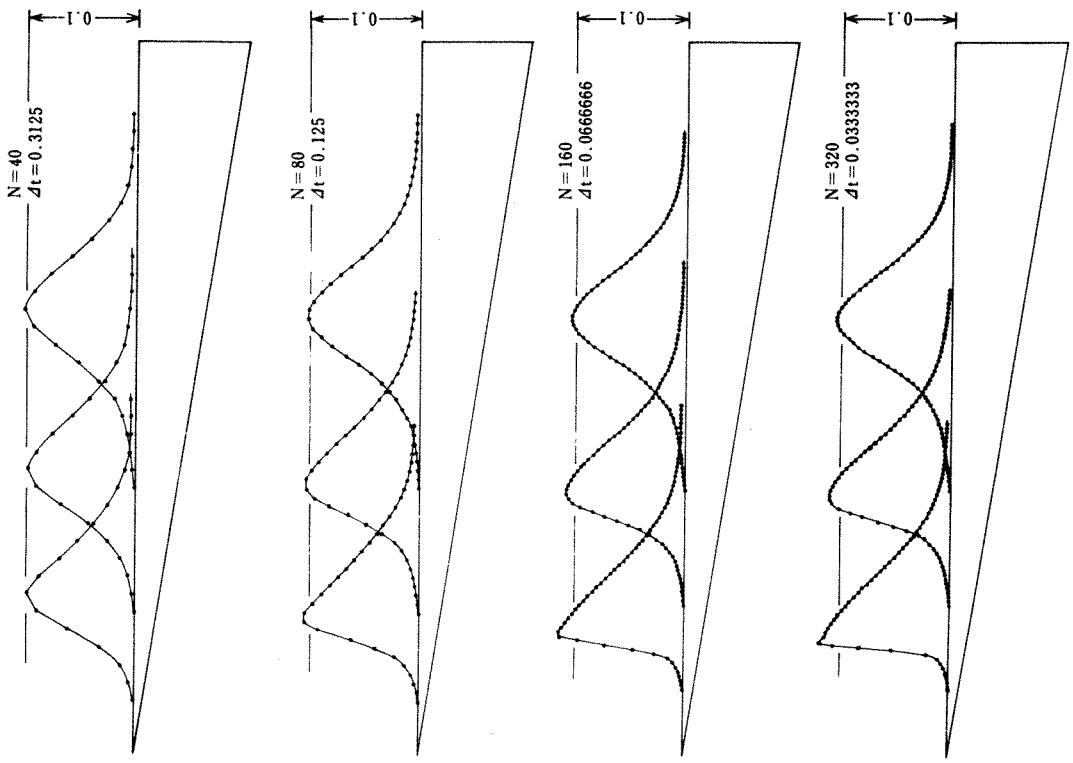

Figure 4. Computed water elevation by the scheme $e = 0{\cdot}8$

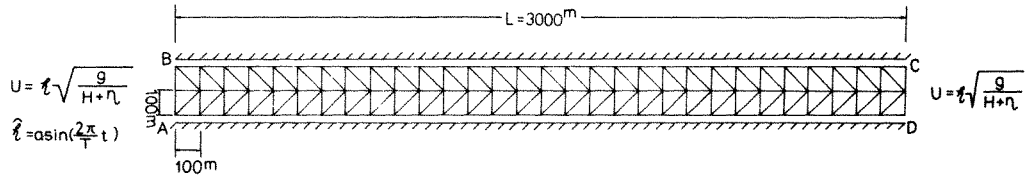

Figure 6. Finite element idealization and boundary conditions

In Figure 5, the computed results are illustrated for the case when $N = 320$ and $e = 0{\cdot}8$ for various time increments Δt. With a rather long time increment (e.g. $\Delta = 0{\cdot}076923$ or $0{\cdot}05$), the computation is unstable. The selection of the time increment rests on the rule that a suitable time increment is the largest value within the limit that a stable computation can be performed. In this example, $\Delta t = 0{\cdot}03333$ seems to be a suitable value.

The second example is the computation of the propagation of a sinusoidal wave. Figure 6 represents the finite element idealization and the specified boundary conditions. The total length of the channel L is 3000 m, while the minimum length of a finite element Δx is 100 m. The depth of the channel is assumed as 10 m. At the boundary A–B, the water elevation is given as

$$\hat{\zeta} = a \sin\left(\frac{2\pi}{T} t\right) \tag{43}$$

where $a = 0{\cdot}5$ m and $T = 300$ sec. The wave expressed by equation (43) corresponds to the case where the wave length is almost equivalent to the channel length L. At the boundary A–B and C–D, a progressive wave condition, i.e.

$$u = \zeta \sqrt{\frac{g}{H + \zeta}} \tag{44}$$

is considered, where H and g are water depth and acceleration due to gravity, respectively. Using the boundary conditions expressed by the equations (43) and (44), water elevation computed at the boundary C–D must be coincident with the one at the boundary A–B, i.e. $\hat{\zeta}$. The ratio of the computed water elevation at the boundary C–D to the specified water elevation at the boundary A–B is plotted in Figure 7 by the use of various selective lumping

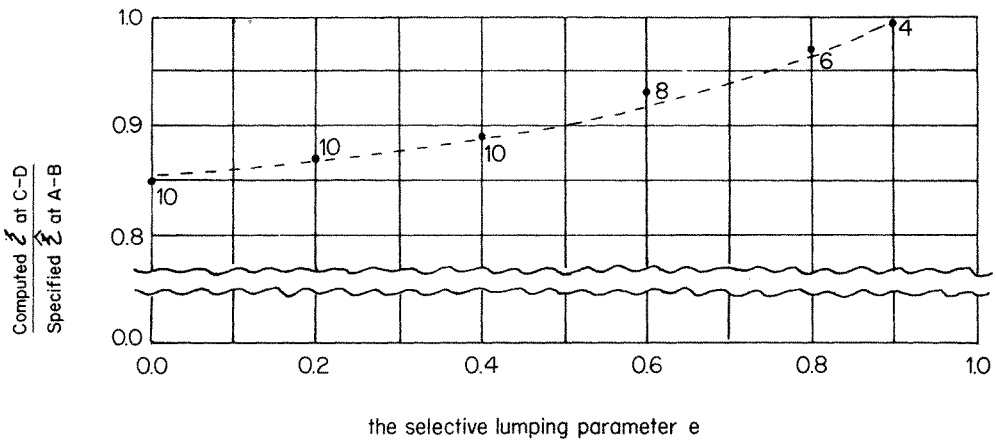

Figure 7. Ratio of computed and specified water elevations

parameters e. The choice of the time increment Δt for each selective lumping parameter is independent and is made according to the stability condition expressed in equation (42). The time increment Δt is chosen as long as possible whilst the computations are stable. The time increment used is also plotted in Figure 7.

The ratio has been computed using the value after the quasi-steady state has been reached. In the case when $e = 0{\cdot}0$ and $\Delta t = 10$ sec, the ratio of the computed water elevation to the specified value is 0·85. On the other hand, in the case when $e = 0{\cdot}8$ and $\Delta t = 6$ sec, the ratio is 0·97. Moreover, in the case when $e = 0{\cdot}9$ and $\Delta t = 4$ sec, the ratio exceeds. 0·99. From the results shown in Figure 7, the following can be concluded: (i) The original scheme includes a significant numerical damping effect if the finite element idealization is insufficient; (ii) The numerical damping effect can be reduced by using the selective lumping technique; (iii) The lumping parameter can be chosen between $e = 0{\cdot}8$ and $e = 0{\cdot}9$. It is necessary that the time increment Δt be shorter than that used in the original scheme.

TIDAL COMPUTATION OF OSAKA BAY

The tidal current flow computation of Osaka Bay has been computed and compared with the observed data measured by the Maritime Safety Agency of Japan.[67] The finite element idealization used in the computation is shown in Figure 8. The total number of nodal points and elements are 609 and 1055, respectively. Along the coastline, the normal velocity to the coast is assumed zero. The tidal elevations at the boundaries are specified as follows.

$$\hat{\zeta} = a \sin\left(\frac{2\pi}{12{\cdot}00\ \text{hr.}} t - \alpha\right)$$

where a and α are listed in Table I.

The computed velocity at high tide plus 3 hours is presented in Figure 9. The solid arrowed lines show the computed velocity and the dashed lines the observed velocity. At the Akashi Strait, the observed velocity attains values up to 3·00 m/sec. The corresponding computed velocity is 3·1 m/sec. Both results show quite reasonable agreement. In this computation, the selective lumping parameter $e = 0{\cdot}92$ and the time increment $\Delta t = 40$ sec. The observed velocity is the value measured at 2 m below the water surface. Figure 10 is the comparison between computed and observed velocity at low tide plus 3 hours. The results also exhibit good agreement.

Figure 11 illustrates the tidal residual flow computed by averaging the computed velocity at each time step over 25 hours and one compared with the observed data. The total circulation pattern as calculated is reasonably well in agreement with observed values. Two dominant circulations can be seen in the residual flow pattern of the observed velocity. On the other hand, the computed velocity shows the one distinct clockwise circulation. This discrepancy seems to be caused by the fact that the observed results include the circulation induced by the factors other than tide—such as wind, river flow and the difference of salinity density and temperature. The ratio of the computed velocity at the midpoint in the Akashi Strait divided by the observed velocity at the same point versus the selective lumping parameter is shown in Figure 12. The maximum velocity observed is 2·7 m/sec at high tide plus 3 hours. From the figure, it can be seen that in this case the selective lumping parameter is chosen to be 0·93 and shows that the computed velocity is coincident with the observed velocity. On the other hand, in this case, the time increment that must be used is 0·58 Δt_1, where Δt_1 is the time increment which was used in the case when $e = 0{\cdot}0$. In conclusion, it is

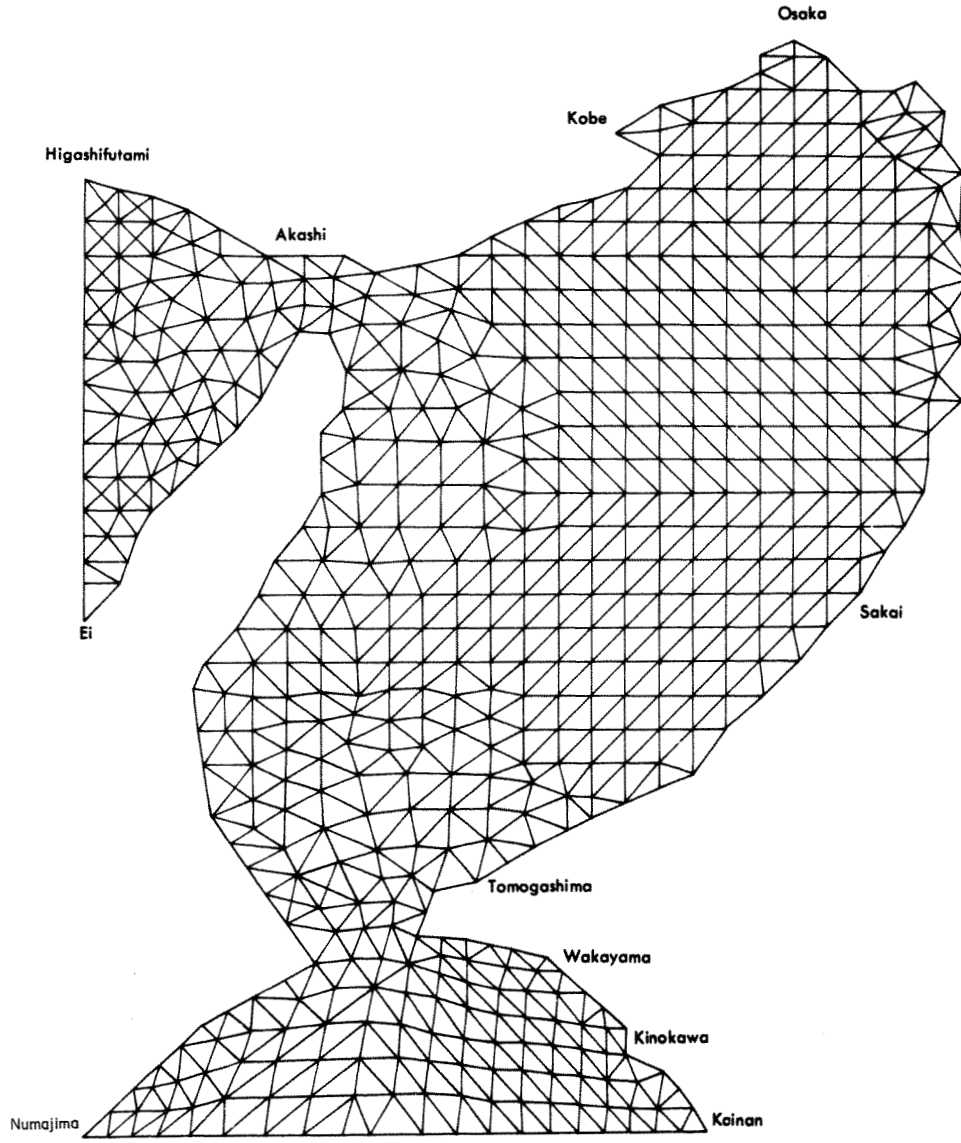

Figure 8. Finite element idealization of Osaka Bay

Table I

	Higashifutami	Ei	Numajima	Kainan
a	0·2846 m	0·3339 m	0·6286 m	0·6608 m
α	294·64 deg.	327·06 deg.	179·80 deg.	188·19 deg.

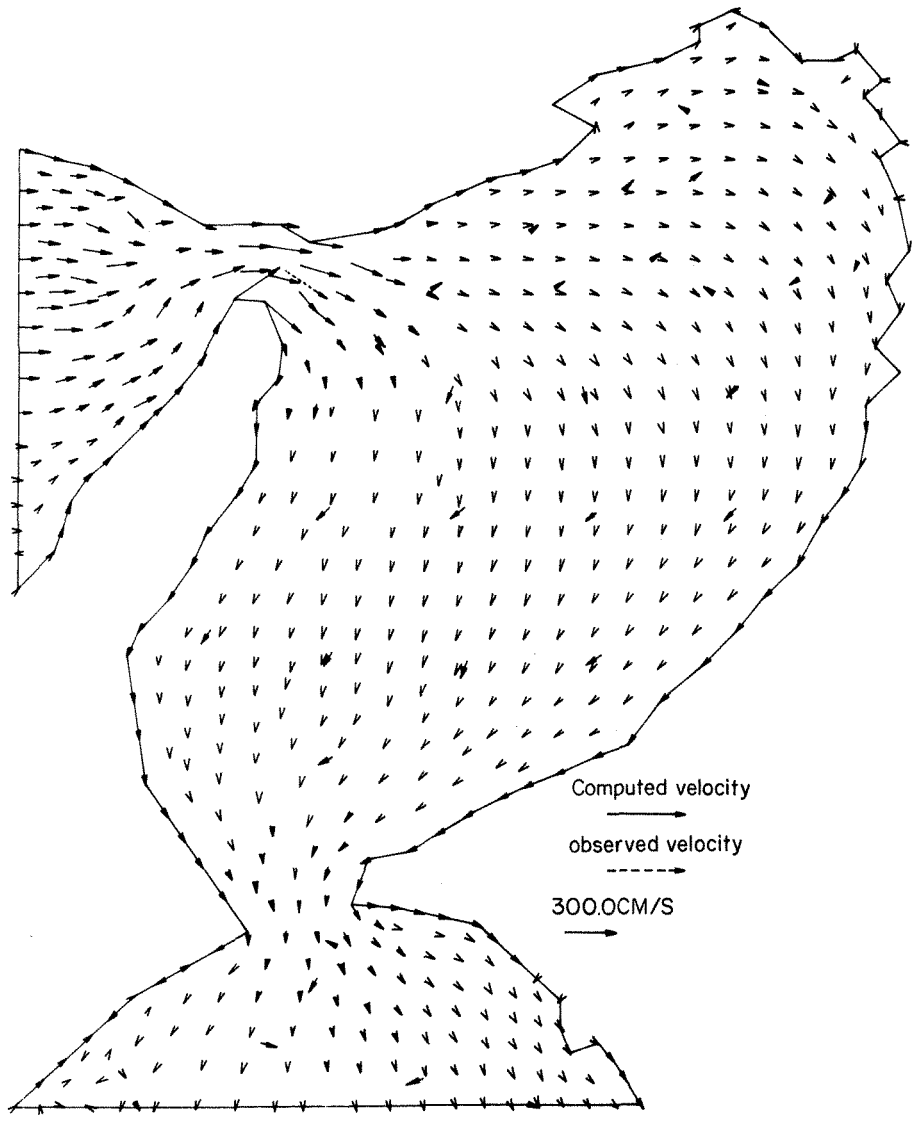

Figure 9. Computed and observed velocity at high tide plus 3 hours (2 m below water surface)

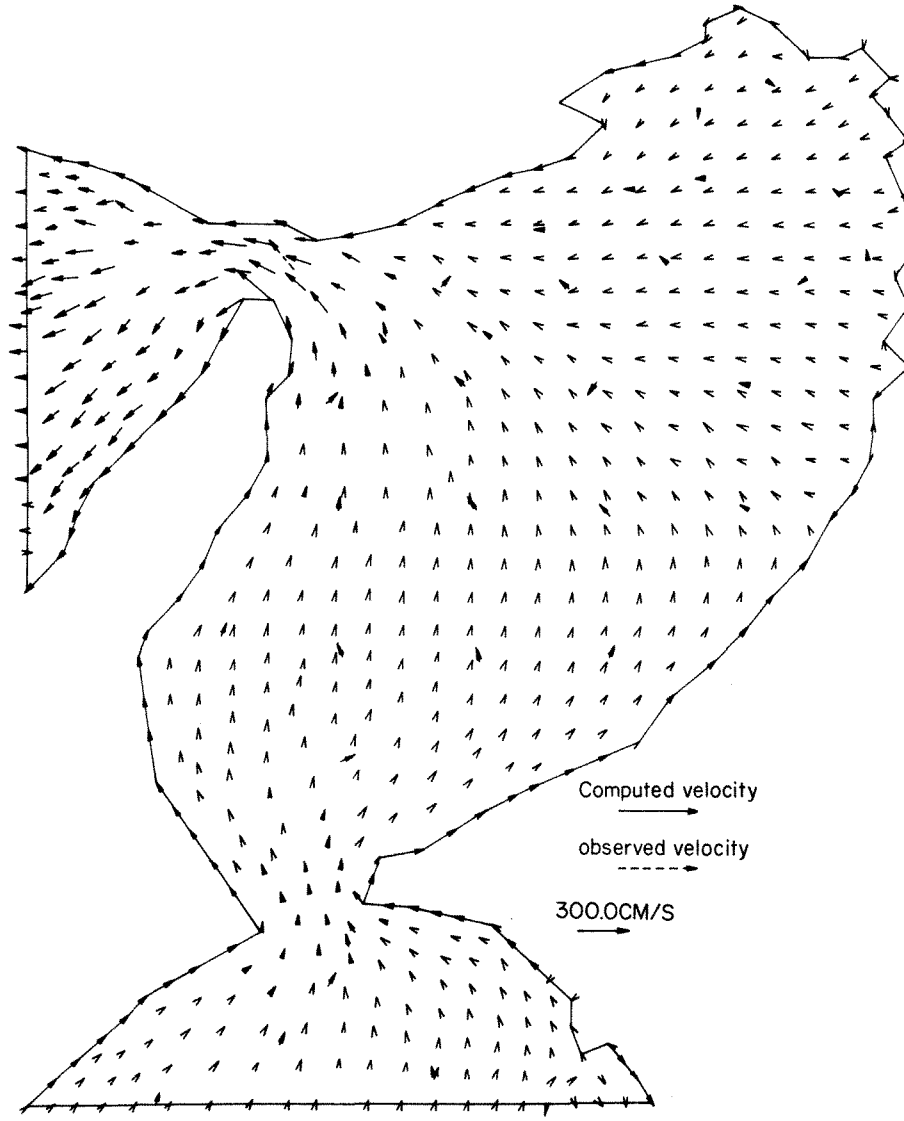

Figure 10. Computed and observed velocity at low tide plus 3 hours (2 m below water surface)

necessary to use the selective lumping parameter e larger than 0·85. Corresponding to this, the time increment could be shorter than that in the original scheme. The computations of this model have been carried out in association with the Port and Harbor Research Insititute, Ministry of Transport, Japan.[68]

TIDAL COMPUTATION OF YATSUSHIRO BAY

The tidal current flow of Yatsushiro Bay includes the tidal shoal. The mean tide observed at Yatsushiro City located at the coastline of Yatsushiro Bay shows that the half-diurnal tide is predominant rather than the diurnal tide. Along the coastline, there are several areas at

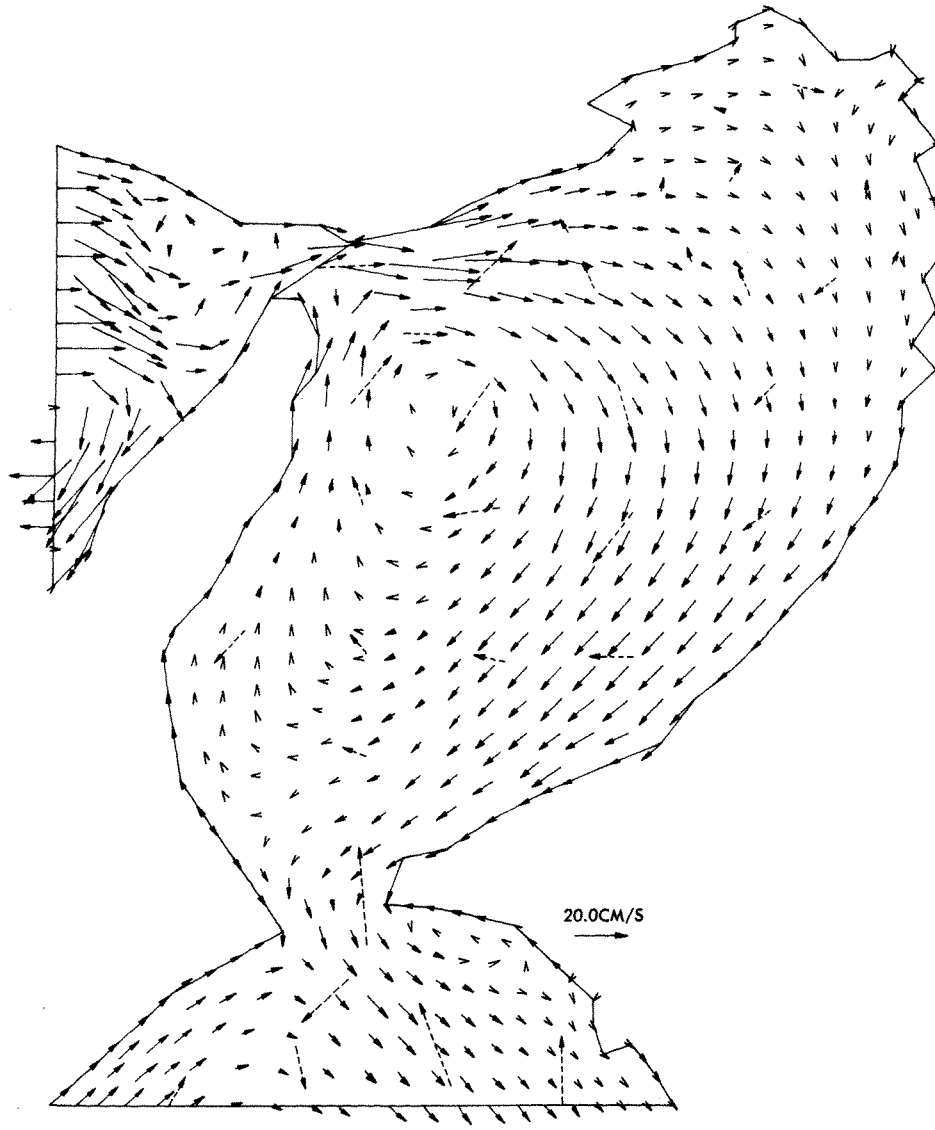

Figure 11. Computed and observed residual current velocity

which the sea bed is exposed at low tide. Therefore, computations have to be carried out which include the exposed sea bed, which can be deduced from the following equations,

if $h = H + \zeta \geq 0$ then the bed is exposed, and

if $h = H + \zeta < 0$ then the bed is under water,

where H is the water depth and ζ is the water elevation; both are computed from the mean sea level.

Using the triangular finite element, the variable definition at each element has been carried out according to the following rules. For each nodal point i of the finite element, water depth H_i, water elevation ζ_i, both components of current velocity u_i, v_i will be given.

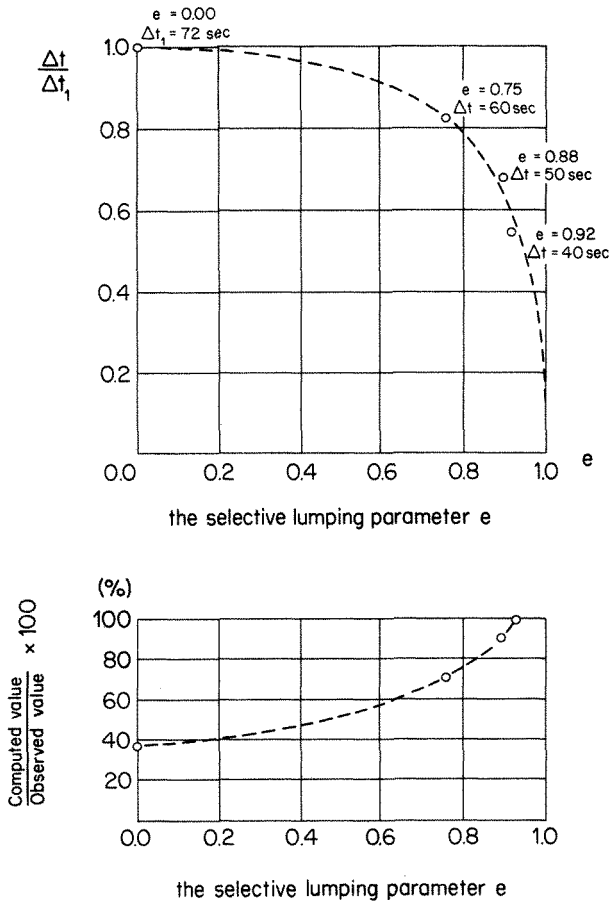

Figure 12. Ratio of computed and observed velocities and time increment employed in the computation

The total water depth $h_i = H_i + \zeta_i$ can be computed. The computation can be characterized by the following,

(i) all nodal values of h_i are $h_i > 0$,

(ii) at least one value of h_i is $h_i > 0$ and the rest of h_i are $h_i < 0$, and

(iii) all values of h_i are $h_i < 0$.

In case (i), the element under consideration is under water. In case (ii), at the nodal point at which $h_i > 0$, the water elevation and current velocity will be computed and at the nodal point at which $h_i < 0$, the water elevation will be computed but the current velocity will be treated as zero. In case (iii), the element is on the exposed sea bed and will be omitted from the computation.

Figure 13 represents the finite element idealization of Yatsushiro Bay. The total numbers of nodal points and finite elements are 759 and 1279, respectively. The bed topography is shown in Figure 14. The tidal elevations specified at the boundaries, A–B, C–D, E–F, G–H are expressed generally as

$$\zeta = (M_2 + S_2) \sin\left(\frac{2\pi}{12 \text{ hour}} t\right)$$

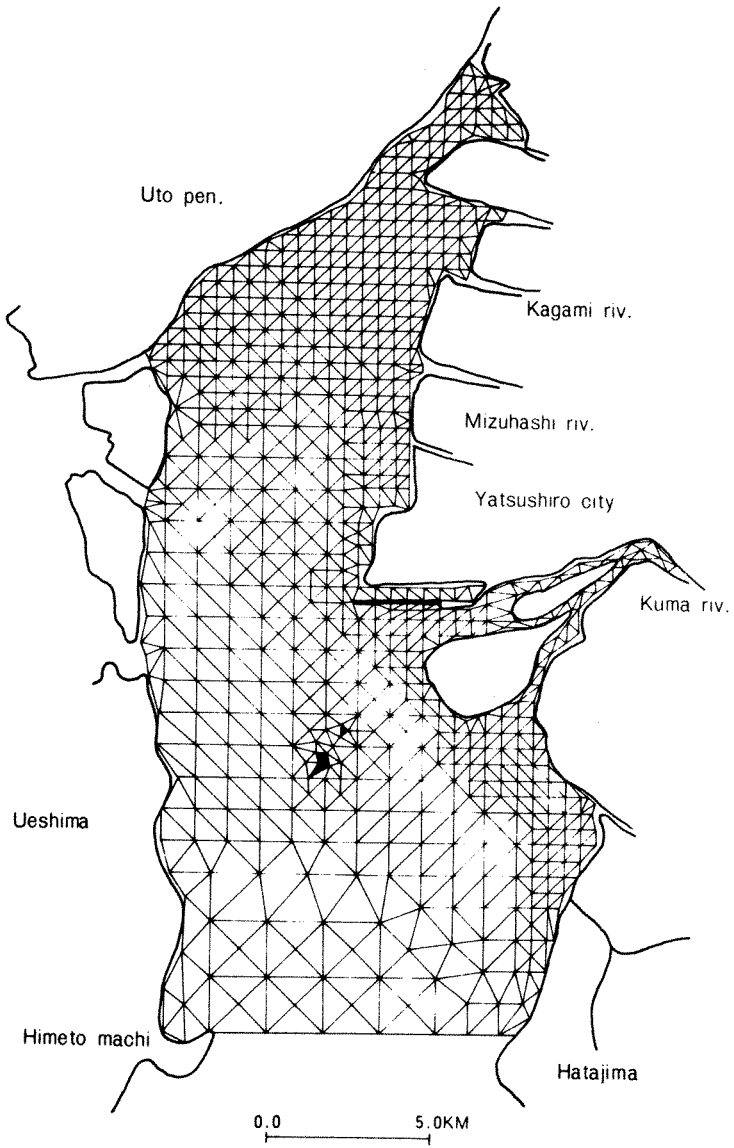

Figure 13. Finite element idealization of Yatsushiro Bay

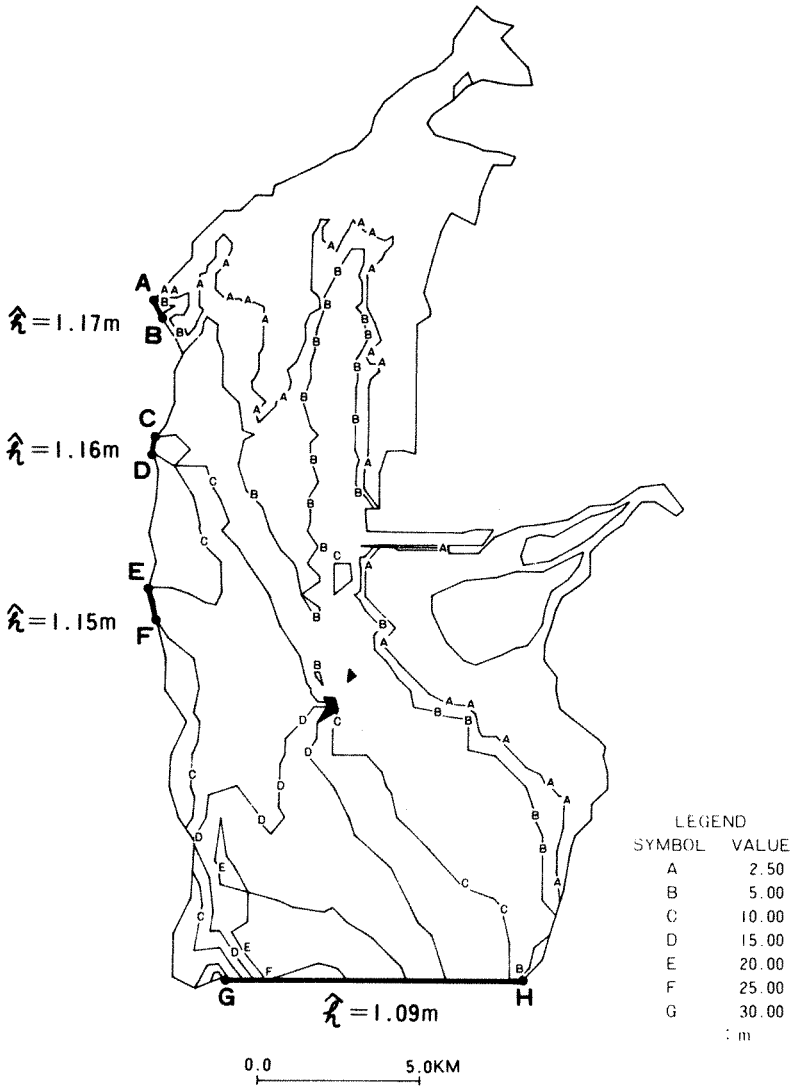

Figure 14. Water depth and boundary conditions

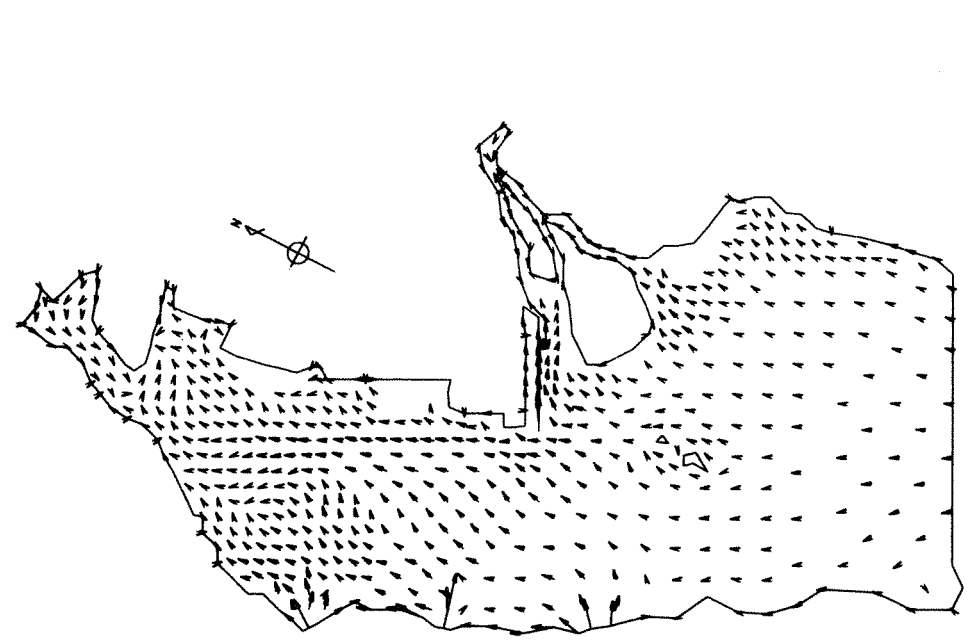

Figure 16. Computed velocity at low tide plus 3 hours

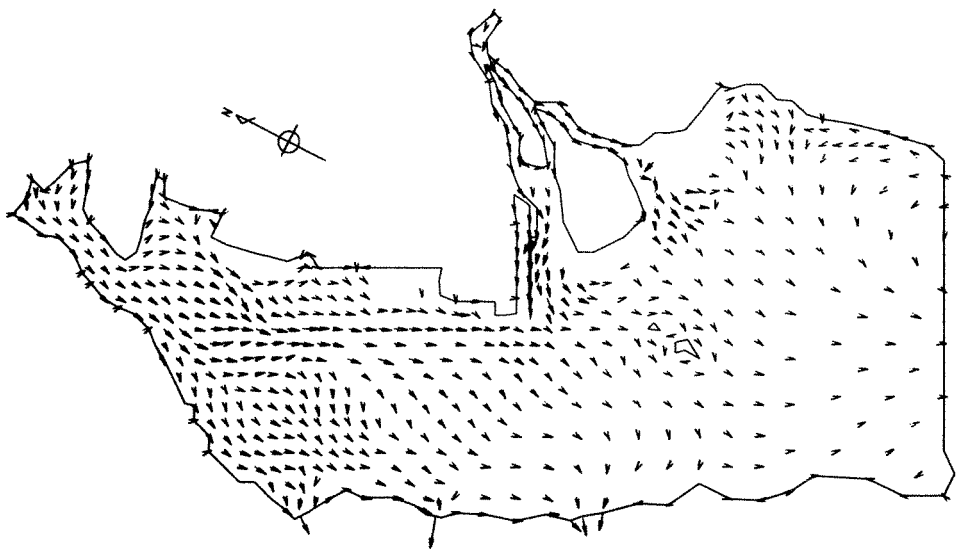

Figure 15. Computed velocity at low tide

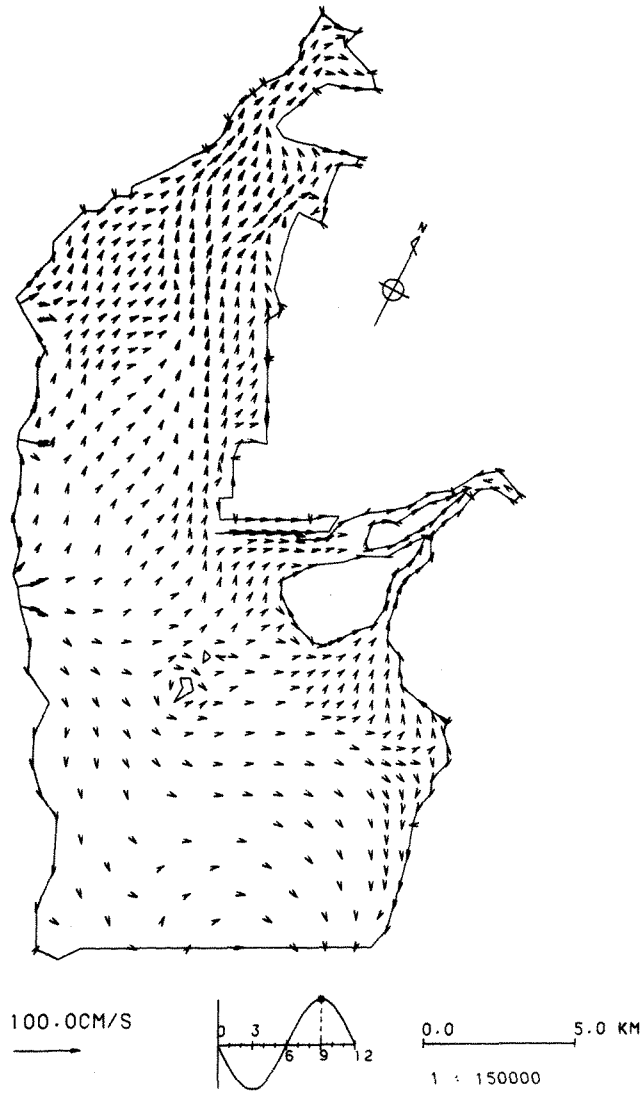

Figure 17. Computed velocity at high tide

where the tide of M_2+S_2 is shown in Figure 14. Along the coastline, the normal velocity to the coast is assumed to be zero. The turbulent eddy viscosity A_l is assumed to be $5{\cdot}0\ m^2/sec$ and the bottom friction is

$$\frac{1}{C^2}=\frac{n^2}{H^{1/3}}$$

where H is water depth and $n=0{\cdot}05\ m^{-1/3}$ sec.

The computed velocity and tidal shoal are illustrated in Figures 15–18. In Figure 15, the computed velocity at low tide is shown. It can be clearly seen that tidal flats are developed along the coastline. In Figure 16, the computed velocity at low tide plus 3 hours is plotted. The numerical results show the tidal shoal is disappearing. Figure 17 illustrates the computed

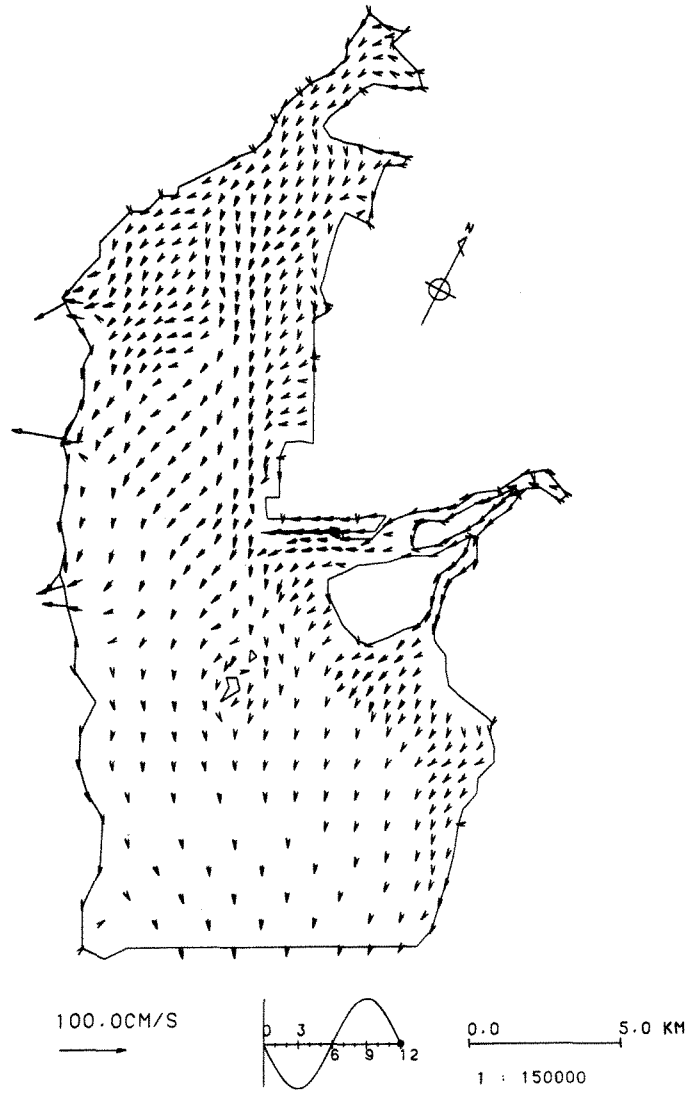

Figure 18. Computed velocity at high tide plus 3 hours

velocity at high tide. All the shoals are under water. Figure 18 represents the computed velocity at high tide plus 3 hours. It is seen that the shoal is exposed. The maximum velocity computed is 40 cm/sec. These numerical results have been applied to the water quality prediction analysis of Yatsushiro Port. The computations of this model have been carried out in association with the government of Kumamoto Prefecture, Japan.

ACKNOWLEDGEMENTS

The authors wish to express their sincere gratitude to Professor O. C. Zienkiewicz for his earnest discussions with the first author who stayed at the University College of Swansea in

1978. The original computer program was coded by Mr. Shohei Nakazawa, former research associate of Chuo University and now of the University College of Swansea. The computation in this paper was carried out with the collaboration of Messrs. Ken'ichi Hasegawa, Toshio Nishida, Mitsuo Kobayashi, Shin'ichi Nakane, Tatsuya Maehara, Sadao Harayama, Jun'ichiro Matsuyama (Unic Corporation) and Shuichi Kodaka (Chuo University) using the PRIME 750 of Unic Corporation, FACOM 230–48S of Chuo University and HITAC 8800/8700 of the University of Tokyo.

REFERENCES

1. K. P. Holz and H. Hennlich, 'Numerical experiences from the computation of tidal waves by the finite element method', in *Finite Elements in Water Resorces* (Eds. Pinder *et al.*), Pentech Press, 1976, pp. 419–431.
2. K. P. Holz and D. Withum, 'Finite element applications for transient processes in estuaries', in *Formulation and Computational Algorithm in Finite Element Analysis* (Eds. Bath *et al.*), M.I.P. Press, 1976, pp. 917–957.
3. F. D. L. Young and J. A. Liggett, 'Transient finite element shallow lake circulation', *Proc. ASCE* **103** (HY2), 109–121 (1977).
4. B. M. Jamart and D. F. Winter, 'Finite element solutions in Fourier Space, with application to Knight Inlet, British Columbia', (Eds. Norrie *et al.*), *3rd Int. Conf. Finite Element Methods in Flow Problems*, 103–112 (1980).
5. B. M. Jamart and D. F. Winters, 'A new approach to the computation of tidal motions in estuaries' in *Hydrodynamics of Estuaries and Fjords* (Ed. Nichoul), North-Holland, 1978, pp. 261–281.
6. M. Kawahara and K. Hasegawa, Finite element analysis of two-layered tidal flow', in *Applications of Computer Methods in Engineering* (Ed. Wellford), University of Southern California, 1977, pp. 1357–1366.
7. M. Kawahara, K. Hasegawa and Y. Kawanago, 'Periodic tidal flow analysis by finite element perturbation method', *Comp. Fluid.*, **5,** 175–189 (1977).
8. M. Kawahara and K. Hasegawa: 'Periodic Galerkin finite element method of tidal flow', *Int. J. num. Meth. Engng*, **12,** 115–127 (1978).
9. M. Kawahara, M. Morihira, S. Kataoka and K. Hasegawa, 'Periodic finite elements in two-layer tidal flow', *Int. j. numer. methods fluids*, **1,** 45–61 (1981).
10. C. E. Pearson and D. F. Winters, 'On the calculation of tidal currents in homogeneous estuaries', *J. Phys. Ocean.*, **7,** 520–531 (1977).
11. G. Warzee and M. A. Sterling, 'Application of the finite element method to periodic tidal computation', *Proc. 3rd Int. Conf. Finite Elements in Water Resources* (Eds. S. Y. Wang *et al.*) (1980).
12. C. L. Provost, A. Poncet and G. Rougier, 'Finite element computation of some tidal spectral components', (Eds. S. Y. Wang *et al.*), *Proc. 3rd Int. Conf. Finite Elements in Water Resources* (1980).
13. A. J. Baker, M. O. Soliman and D. W. Pepper, 'A time-split finite element algorithm for environmental release prediction', in *Finite Elements in Water Resources* (Eds. Brebbia *et al.*), 1978, pp. 4.53–4.65.
14. A. J. Baker and M. O. Soliman, 'Analysis of a finite element algorithm for numerical predictions in water resources research', in *Finite Elements in Water Resources* (Eds. Wang *et al.*), the University of Mississippi, 1980.
15. C. A. Brebbia and P. W. Partridge, 'Finite element models for circulation studies', in *Mathematical Models for Environmental Problems* (Ed. Brebbia), Pentech Press, 1975, pp. 141–159.
16. C. A. Brebbia and P. W. Partridge, 'Finite element simulation of water circulation in the North Sea', *Appl. Math. Mod.*, **1,** 101–107 (1976).
17. P. W. Partridge and C. A. Brebbia, 'Quadratic finite elements in shallow water problems', *Proc. ASCE*, **102,** No. HY9, 1299–1313 (1976).
18. R. T. Cheng and R. A. Walters, 'Some finite element applications in environmental hydrodynamics', *U.S.–Japan Seminar on Interdisciplinary Finite Element Analysis* (Eds. Abel *et al.*), Cornell University, p. A9 (1978).
19. R. A. Walters and R. T. Cheng, 'A two dimensional hydrodynamic model of tidal estuaries', in *Finite Elements in Water Resources* (Eds. Brebbia *et al.*), 1978, pp. 2.3–2.21.
20. R. A. Walters and R. T. Cheng, 'Calculations of estuarine residual currents using the finite element method', *Proc. 3rd Int. Conf. in Finite Element Methods in Flow Problems* (Eds. D. H. Norrie), **II**, 60–69 (1980).
21. J. J. Connor and G. C. Wang, 'Finite element modelling of hydrodynamic circulation', in *Numerical Methods in Fluid Dynamics* (Eds. Brebbia *et al.*), Pentech Press, 1977, pp. 355–387.
22. W. G. Gray, 'An efficient finite element scheme for two dimensional surface water computation' in *Finite Elements in Water Resources* (Eds. Pinder *et al.*), Pentech Press, 1977, pp. 433–449.
23. W. G. Gray and D. R. Lynch, 'Time stepping schemes for finite element tidal model computations', *Advances Water Resources*, **2,** 83–95 (1977).
24. D. R. Lynch and W. G. Gray, 'Finite element simulation of shallow water problems with moving boundaries', in *Finite Elements in Water Resources* (Eds. Pinder *et al.*), 1978, pp. 2.23–2.42.

25. W. G. Gray, 'Two dimensional flow modelling by finite elements', *Proc. 3rd Int. Conf. Finite Elements in Water Resources* (Eds. S. Y. Wang *et al.*), (1980).
26. G. Grotkop, 'Finite element analysis of long-period water waves', *Comp. Meth. Appl. Mech. Engng.*, **2,** 147–157 (1973).
27. B. Herrling, 'Finite element model for estuaries with inter-tidal flats', *Proc. 15th Coastal Engng Conf. Honolulu,* ASCE 3396–3415 (1976).
28. B. Herrling, 'Tidal computation in the Elbe estuary with a coupled FE model', *Proc. 3rd Int. Conf. Finite Elements in Water Resources* (Eds. S. Y. Wang. *et al.*), (1980).
29. K. P. Holz, 'Finite elements, a flexible tool for modelling estuarine processes', in *Mathematical Modelling of Estuarine Physics* (Eds. Sündermann *et al.*), Springer-Verlag, 1980.
30. K. P. Holz and G. Nitsche, 'Tidal wave analysis for estuaries with intertidal flats', *Proc. 3rd Int. Conf. Finite Elements in Water Resources* (Eds. Wang *et al.*), (1980).
31. N. D. Katopodes, 'Finite element model for open channel flow near critical conditions', *Proc. 3rd Int. Conf. Finite Elements in Water Resources* (Eds. Wang. *et al.*), (1980).
32. I. P. King and W. R. Norton, 'Recent application of RMA's finite element models for two dimensional hydrodynamics and water quality', in *Finite Elements in Water Resources* (Eds. Pinder *et al.*), 1978, pp. 2.81–2.99.
33. R. A. MacArthur and W. R. Norton, 'Application of the finite element method to vertically stratified hydrodynamic flow and water quality', *Proc. 3rd Int. Conf. Finite Elements in Water Resources* (Eds. Wang *et al.*), (1980).
34. A. Moult, 'An upwind finite element formulation for convention or buoyancy dominated flows in rivers, bays and estuaries', *Proc. 3rd Int. Conf. Finite Elements in Water Resources* (Eds. Wang *et al.*), (1980).
35. Y. Matsuda, 'A water pollution prediction system by the finite element method', in *Finite Elements in Water Resources* (Eds. Pinter, *et al.*), 1978, pp. 2.101–2.117.
36. U. Meissner, 'Discretization and time integration schemes for hydrodynamical finite element models', in *Formulations and Computational Algorithm in Finite Element Analysis* (Eds. Bath *et al.*), 1976, pp. 1012–1038.
37. W. G. Platzman, 'Normal modes of the world ocean, part I: Design of a finite element barotropic model', *J. Phys. Ocean.*, **8,** 323–343 (1978).
38. A. N. Staniforth and R. W. Daley, 'A finite element formulation for the vertical discretization of sigma-coordinate primitive equation model', *Mon. Wea. Rev.*, **105,** 1108–1118 (1977).
39. A. N. Staniforth and H. L. Mitchell, 'A semi-implicit finite-element barotropic model', *Mon. Wea. Rev.*, **105,** 154–169 (1977).
40. A. N. Staniforth and H. L. Mitchell, 'A variable resolution finite element technique for regional forecasting with the primitive equation', *Mon. Wea. Rev.*, **106,** 439–447 (1978).
41. J. Sündermann, 'Computation of barotropic tides by the finite element method', in *Finite Elements in Water Resources* (Eds. Pinder *et al.*), Pentech Press, 1976, pp. 451–467.
42. M. Rahman, D. Prandle, L. Spraggs and V. Argintaru, 'Numerical methods for tidal propagation applied to a hybrid model of the Bay of Fundy', *Proc. 3rd Inf. Conf. Finite Elements in Water Resources* (Eds. S. Y. Wang *et al.*), (1980).
43. T. Y. Su and S. Y. Wang, 'Depth-Averaging models of river flows', *Proc. 3rd Int. Conf. Finite Elements in Water Resources* (Eds. S. Y. Wang *et al.*), (1980).
44. M. Thienpont and J. Berlamont, 'A finite element solution of depth averaged two dimensional Navier–Stokes equations in river and channels', *Proc. 3rd Inf. Conf. Finite Elements in Water Resources* (Eds. S. Y. Wang *et al.*), (1980).
45. T. Tanaka, T. Hirai and T. Katayama, 'Finite element applications to lake circulations and diffusion problems in Lake Biwa', in *Finite Element Methods in Flow Problems* (Eds. Gallagher *et al.*), I.C.C.A.D. (1976).
46. T. Tanaka and T. Katayama, 'Finite element analysis of typhoon surge in Ise Bay', *U.S.—Japan Seminar on Interdisciplinary Finite Element Methods* (Eds. Abel *et al.*), Cornell University, p. J11 (1978).
47. T. Tanaka, Y. Ono and T. Ishise, "The ocean boundary value problems in ocean dynamics by finite elements', *Proc. 3rd Int. Conf. on Finite Elements in Water Resources* (Eds. S. Y. Wang *et al.*), (1980).
48. C. Taylor and J. M. Davis, 'Tidal and long wave propagation—a finite element approach', *Comp. Fluid.*, **3,** 125–148 (1975).
49. C. Taylor and J. M. Davis, 'Tidal propagation and dispersion in estuaries', in *Finite Elements in Fluids Vol.* 1, Wiley, Chichester, 1975, pp. 95–118.
50. M. J. P. Cullen, 'A simple finite element method for meteorological problems', *J. Inst. Math. Appl.*, **11,** 15–31 (1973).
51. M. J. P. Cullen, 'Integration of the primitive variable equations on a sphere using the finite element method', *Quart. J. R. Met. Soc.*, **100,** 555–562 (1974).
52. M. J. P. Cullen, 'A finite element method for non-linear initial value problems', *J. Inst. Math. Appl.*, **13,** 233–247 (1974).
53. M. J. P. Cullen, 'The application of finite element methods to primitive equation of fluid motion', in *Finite Elements in Water Resources* (Eds. Pinder *et al.*), Pentech Press, 1977, pp. 4.231–4.245.
54. H. Kanayama and K. Ohtsuka, 'Finite element analysis on the tidal current and the COD distribution of Mikawa Bay', *Proc. IFAC Symp. Environmental Systems Planning Design and Control* (1977).

55. M. Kawahara, N. Takeuchi and T. Yoshida, 'Two step explicit finite element method for tsunami wave propagation analysis', *Int. J. num. Meth. Engng*, **12,** 331–351 (1978).
56. M. Kawahara, S. Nakazawa, S. Ohmori and K. Hasegawa, 'Tsunami wave propagation analysis by the finite element method', in *Finite Element Methods in Water Resources* (Eds. C. A. Brebbia *et al.*), (1978), pp. 2.130–2.150.
57. M. Kawahara and S. Nakazawa, 'Finite element method for unsteady shallow water wave equation', *U.S.–Japan Seminar on Interdisciplinary Finite Element Methods* (Eds. Abel *et al.*), Cornell University (1978).
58. M. Kawahara, 'On finite element methods in shallow water long wave flow analysis', in *Computational Methods in Nonlinear Mechanics* (Ed. J. T. Oden), North-Holland, 1980.
59. M. Kawahara and T. Yokoyama, 'Finite element method for direct runoff flow', *Proc. ASCE*, **106,** No. HY4, 519–534 (1980).
60. M. Kawahara, S. Nakazawa, S. Ohmori and T. Takagi, "Two step explicit finite element method for storm surge propagation analysis', *Int. J. num. Meth. Engng*, **15,** 1129–1148 (1980).
61. S. Nakazawa, D. W. Kelly, O. C. Zienkiewicz, I. Christie and M. Kawahara, 'An analysis of explicit finite element applications for shallow water equations', *Proc. 3rd Int. Conf. Finite Element Methods in Flow Problems* (Eds. Norrie *et al.*), **II,** 1–12 (1980).
62. M. Kobayashi, K. Nakata and M. Kawahara, 'A three-dimensional multi-levelled finite element model for density current analysis', *Proc. 3rd Int. Conf. Finite Element Methods in Flow Problems*, **II,** 80–92 (1980).
63. J. F. Cochet, D. Dhatt and G. Touzot, 'Comparison of explicit and implicit methods applied to finite element models of tidal problems', *Proc. 3rd Int. Conf. Finite Element Methods in Flow Problems* (Eds. Norrie *et al.*), **II,** 113–122 (1980).
64. H. P. Wang, 'Multi-level finite element hydrodynamic model of Block Island sound', in *Finite Elements in Water Resources* (Eds. Pinder *er al.*), 1975, pp. 469–493.
65. J. D. Wang, 'Real time flow in unstratified shallow water flow', *Proc. ASCE*, **104,** No. WW1, 53–68 (1978).
66. J. D. Wang, 'Analysis of tide and current meter data for model verification', in *Mathematical Modelling of Estuarine Physics*, (Eds. Sündermann *et al.*), Springer-Verlag, 1980.
67. N. Yamada, 'Tidal flow of Osaka Bay', *Reports of Flow in Channel*, **96,** 23–31 (1976), in Japanese.
68. K. Murakami, M. Morikawa, S. Yokota and T. Horie, 'Finite element analysis on flow and substance dispersion', *Technical Note*, Port and Harbor Research Institute (in Japanese), June (1981).